



HAL
open science

Unrest at Cayambe Volcano revealed by SAR imagery and seismic activity after the Pedernales subduction earthquake, Ecuador (2016)

P.A. Espín Bedón, Laurence Audin, M.-P. Doin, Virginie Pinel, E. Pathier, P. Mothes, André Garcia, Pablo Samaniego, Pacheco Daniel

► To cite this version:

P.A. Espín Bedón, Laurence Audin, M.-P. Doin, Virginie Pinel, E. Pathier, et al.. Unrest at Cayambe Volcano revealed by SAR imagery and seismic activity after the Pedernales subduction earthquake, Ecuador (2016). *Journal of Volcanology and Geothermal Research*, 2022, 428, pp.107577. 10.1016/j.jvolgeores.2022.107577 . hal-04320288

HAL Id: hal-04320288

<https://uca.hal.science/hal-04320288>

Submitted on 4 Dec 2023

HAL is a multi-disciplinary open access archive for the deposit and dissemination of scientific research documents, whether they are published or not. The documents may come from teaching and research institutions in France or abroad, or from public or private research centers.

L'archive ouverte pluridisciplinaire **HAL**, est destinée au dépôt et à la diffusion de documents scientifiques de niveau recherche, publiés ou non, émanant des établissements d'enseignement et de recherche français ou étrangers, des laboratoires publics ou privés.

Unrest at Cayambe Volcano revealed by SAR imagery and seismic activity after the Pedernales subduction earthquake, Ecuador (2016)

Espín Bedón P.A. (1), Audin L. (2), Doin M-P. (2), Pinel, V. (2), Pathier E. (2), Mothes P. (1), Garcia A. (1), Samaniego P. (1,3), Pacheco D. (4).

(1) Instituto Geofísico – Escuela Politécnica Nacional, Quito, Ecuador

(2) Univ. Grenoble Alpes, Univ. Savoie Mont Blanc, CNRS, IRD, Univ. Gustave Eiffel, ISTerre, 38000 Grenoble, France

(3) Laboratoire Magmas et Volcans, Université Clermont Auvergne-CNRS-IRD, Clermont Ferrand, France

(4) Université Côte d'Azur, CNRS, IRD, Observatoire de la Côte d'Azur, Géoazur, Valbonne, France

Keywords:

Cayambe, volcanic unrest, InSAR time series, seismic swarm, volcano-tectonic interactions

Abstract

For the first time in decades, a sudden increase in seismicity has been observed and monitored at Cayambe volcano in Ecuador, in 2016. This seismic unrest, which occurred a few months after the April 2016, Mw 7.8 Pedernales subduction earthquake, has raised many questions, especially as there is no record of recent eruptions at Cayambe volcano. Here we analyze a time series of 104 images from Sentinel 1 (SAR) data spanning the period 2014-2018 using the NSBAS processing chain in order to quantify surface deformation around this potentially explosive and ice-covered volcano. We evidence a large-scale uplift reaching a maximum mean displacement rate of about 0.44 cm/yr in Line of Sight. This uplift is mainly due to a significant and sudden acceleration of the deformation pattern, focused on the SE flank starting in November 2016. We model this signal as related to magma emplacement at around 6 km depth below the summit, with a sudden volume influx of about 2.6 million m³. The inflation and surface deformation pattern is concomitant in time with two Mw 3 seismic events recorded at Cayambe volcano in November 2016

and is consistent with the location at the summit of the volcano-tectonic (VT) seismic swarm from September 2016 onwards. This VT swarm follows an earlier swarm in June 2016 located on the northern side of the volcano and closer to a western branch of the Chingual-Cosanga-Pallatanga-Puna (CCPP) fault system, that plays a major role in accommodating plate tectonic processes in South America. We thus propose that static stress changes from the Pedernales megathrust earthquake triggered magma ascent below the Cayambe volcano, through reactivation of the CCPP fault system. Finally, volcanic hazards around Cayambe ice-capped volcano, previously dormant for the last 300 years, should be reassessed in light of this recent unrest.

1. Introduction

With the launch of Sentinel satellites initiated in 2014 as part of the Copernicus Program led by the European Space Agency (ESA) remote sensing has entered a new era with data systematically acquired and provided free of charge, thus offering new opportunities for the study of volcanoes and their monitoring (Pinel et al. 2014, Biggs and Pritchard, 2017; Ebmeier et al. 2018; Valade et al. 2019; Biggs and Wright, 2020). In particular, InSAR which combines the Satellite Aperture Radar (SAR) signal acquired from different orbital positions and/or at different times is a well-established and efficient technique to monitor large scale deformation of the Earth's surface at multiple times (Simons and Rosen, 2015; Biggs et al. 2016; Pepe and Calo, 2017). A few processing chains have been implemented to fully take advantage of these new datasets, among them the “New Small Baseline Subset (NSBAS)” processing chain (Doin et al. 2011) dedicated to retrieving the temporal evolution of surface displacement for SAR time series. The combination of an increasing amount of SAR data and improved processing methods is expected to favor subtle signal detection and analysis particularly in such vegetated and topographically active areas as the Andes. Here, we test this new potential by studying surface deformation patterns at Cayambe volcano, in northern Ecuador, which experienced a recent seismic crisis (Butcher et al. 2021).

For regional studies, InSAR is indeed a perfect tool to be applied to the Andes volcanic arc where volcano-tectonic activity mostly induces low magnitude ($M < 4$) local earthquakes and moderate surface deformation, but significant volcanic hazards. This technique will improve the monitoring of broad volcanic areas where a scarce number of field instruments are deployed on volcanoes identified as active with the risk of missing the sudden reactivation of a dormant edifice. It has thus already been applied widely in Latin America allowing detection of surface deformation at 26 volcanic edifices between 2013 and 2017 (Pritchard et al. 2018). No surface displacement had been detected at Cayambe volcano neither during this time period nor between 2006 and 2008, reported in an ALOS data-based survey of Latin American volcanoes (Fournier *et al.* 2010). However, to our knowledge, no detailed

study has been performed mainly because the last known eruption occurred more than two hundred years ago.

The Northern Andes of Ecuador displays one of the most active volcanic areas in the world. The geodynamic setting of the active volcanic arc in Ecuador is characterized by intense activity since the Pleistocene, with at least 21 active volcanoes during the Holocene (e.g., Hall and Beate, 1991; Hall et al., 2018; Bernard and Andrade, 2011; Bablon et al., 2019). Eight of these volcanic edifices have erupted in the last 500 years, and some of which have been active and erupting in recent years: Guagua Pichincha (1999-2001), Tungurahua (1999-2006), Reventador (since 2002), Cotopaxi (2015) and Sangay (since 2018) volcanoes. (<https://www.igeppn.edu.ec/red-de-observatorios-vulcanologicos-rovig>). For the last 10 years, seismic and GPS networks have been deployed over the main hazardous volcanoes in Ecuador (Alvarado et al., 2018; Mothes et al., 2018) as seismicity, in particular Volcano-Tectonic (VT) and Low-Period (LP) events, remains the clearest geophysical signal provided by field instruments of an impending eruption (White and McCausland, 2016, 2019). However the interpretation of seismic swarms during volcanic unrest, despite its huge potential for eruption forecasting, is significantly improved by using additional geodetic datasets (Champenois et al., 2014; Biggs et al., 2016). Surface displacements induced by magma emplacement at depth have been observed at long-lived volcanic edifices in Ecuador, such as Tungurahua, whether during eruptions or inter-eruptive periods (Biggs et al., 2010; Champenois et al., 2014). But, short-term transient deformation signals limited to the area proximal to the summit remain difficult to detect with infrequent satellite observations, or distal ground-based monitoring instruments (Ebmeier et al., 2013).

Cayambe volcano is located at to the northern part of the Eastern Cordillera and its construction has been probably controlled by regional N35° major fault systems that connect to the Chingual-Cosanga-Pallatanga-Puna (CCPP, dextral transcurrent, with compressive components) limit of the North Andean Sliver (Alvarado et al., 2017; Bablon et al. 2019). Significant seismic activity was recorded in the volcano: between 2000 and 2004 (Samaniego et al., 2004) characterised by an increase in VT-type event activity. Also, increase of seismic activity in 2016-2017 as

well as new cracks on the ice cap at the end of 2016 have been reported on Cayambe volcano by Instituto Geofísico - Escuela Politécnica Nacional (IGEPN). Here we analyze the Sentinel 1 descending time series recorded between 2014 and 2018 and compare the surface deformation observed at Cayambe volcano with the seismic activity. We then invert for the magma volume perturbation at depth causing the displacement field recorded at the surface. Based on this particular example, we further discuss both the triggering of volcanic unrest by subduction earthquakes and the potential of systematic processing of Sentinel-1 data to complement field measurements and improve the monitoring of large scale volcanic areas.

2. Cayambe volcano tecto-volcanic context and recent eruptive activity

In Ecuador, volcanoes are distributed within a ~70-120 km-wide area in the high Andes encompassing the volcanic front in the Western Cordillera, the main arc in the Eastern Cordillera, and the back-arc region in the Eastern foothills (Fig. 1). In the northern part of the Eastern Cordillera, the construction of the Cayambe Volcanic Complex (CVC) was controlled by the major CCPP fault system and its related subsidiary NNE faults, which bound the North Andean Sliver (NAS) (Fig. 1, Alvarado et al., 2016; Yepes et al., 2016). The Cayambe volcanic complex (CVC) is located at 0.023° latitude, -77.98° longitude, 60 km northeast of Quito (Ecuador's capital) and 15 km west of Cayambe city (Fig. 1). CVC is composed of an old, extinct western edifice called the 'Viejo Cayambe' and a younger, still active eastern Nevado Cayambe volcano (Samaniego et al., 2005). Nevado Cayambe Volcano is an explosive stratovolcano (Fig. 2) emitting andesitic and dacitic lavas and composed of several domes and summits; the maximum height is 5790 m.a.s.l. (Samaniego et al., 1998; Samaniego et al., 2005). Above 4800 meters elevation a.s.l., the volcano is covered by an important ice cap with an area of approximately 22 km² and which reaches a thickness of 30 to 50 m at the summit (Caceres, 2010).

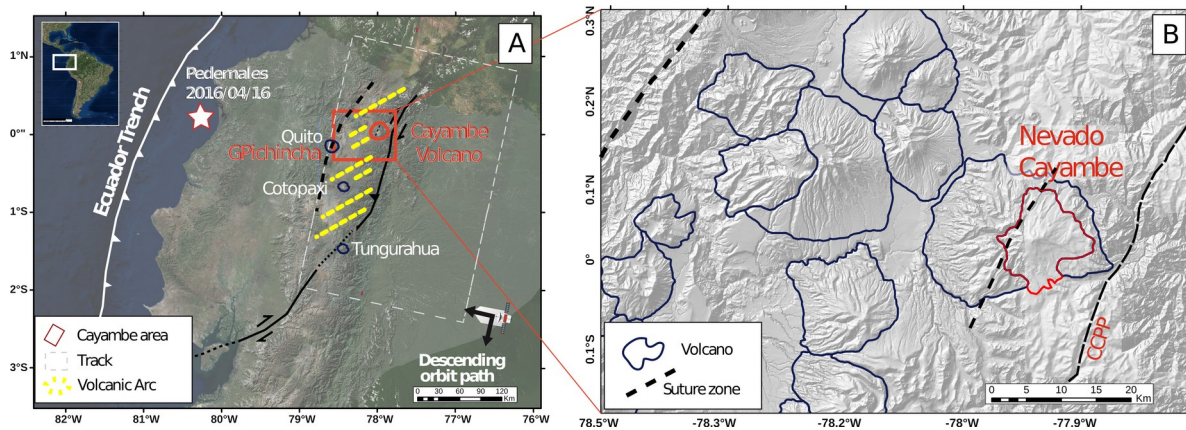


Figure 1. Location of Cayambe Volcano: A) Map of the current Ecuadorian volcanic arc (yellow dashed lines) with recently active volcanoes (last eruption < 20 years, blue circles) and Cayambe Volcano area (red square), b) Inactive volcanoes of the eastern cordillera in the vicinity of Cayambe volcano (from www.igepn.edu.ec) shown on the shaded DEM (Digital Elevation Model). The bold red contour line is for the young Cayambe whereas the surrounding blue contour line is for the older Cayambe volcanic complex. The Chingual-Cosanga-Pallatanga-Puna (CCPP) active faults that limit the North Andean Sliver are shown as solid lines with dashed lines for inherited sutures, partly hidden by the Quaternary volcanic layers.

Nevado Cayambe (NC) is considered an active volcano, whose eruptive activity was characterized by lava dome extrusions, dome collapses, and pyroclastic currents. Based on tephrochronologic studies at least 21 eruptive events have been reported during the last 4000 years, of which the most recent took place between 1785 and 1786 CE (Samaniego et al., 1998)

During the last 20 years, Instituto Geofísico - Escuela Politécnica Nacional (IG-EPN) reported punctual increases in seismic activity related to volcano tectonic events (VT). Such a seismicity increase occurred between 2001 and 2005 (in 2002 ~ 1310 VT events), but quickly returned to the background level without producing surface manifestations or eruptions (Global Volcanism Program, 2006, Report on Cayambe). In 2016 the increase in VT seismic events was stronger in amplitude than previous events, thus motivating the installation of a temporary seismological network to monitor the crisis evolution in case of an upcoming eruption. Additionally, an increase in sulphur emissions in the upper parts of the volcano and the appearance of

new cracks in the ice cap on the highest summit were reported by climbers (Instituto Geofísico - EPN, 2016a, b, c, d and e; Instituto Geofísico - EPN, 2017a and b).

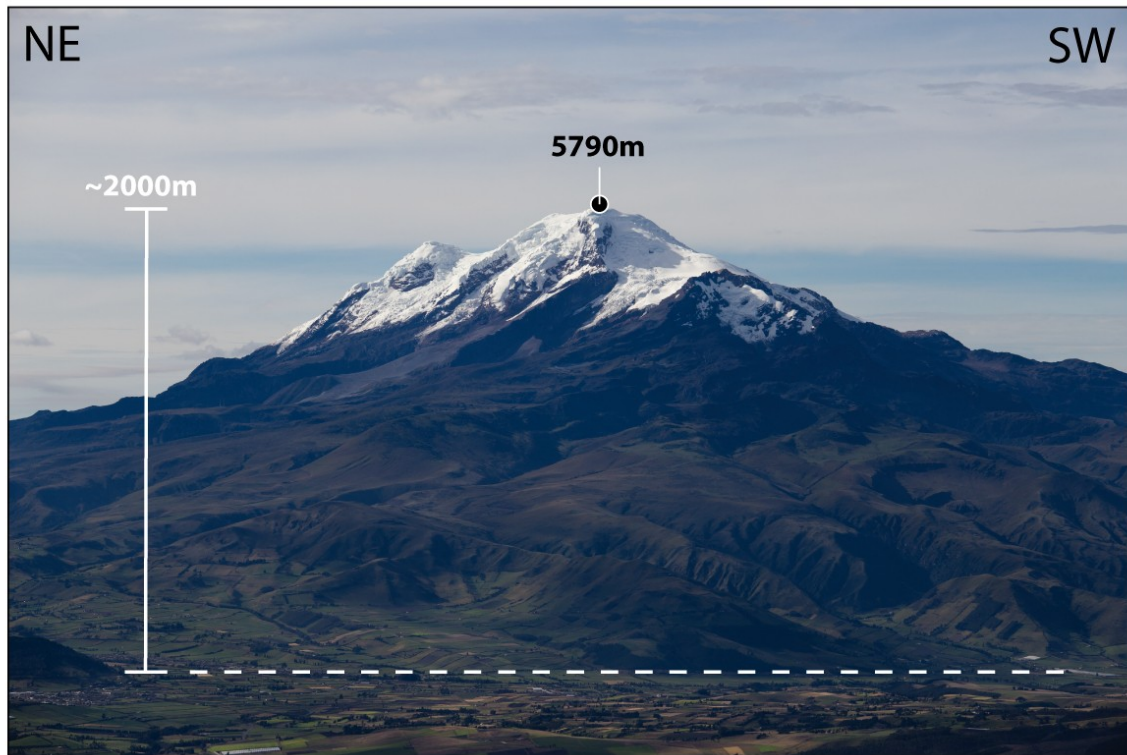


Figure 2. Cayambe volcano. View from the northeast (Photo: Matthieu Perrault, May 2nd, 2015)

3. Recent seismic activity recorded at Cayambe volcano

The Cayambe background seismicity is usually rather low (< 20 events/day and below magnitude 3) and mostly characterized by Long Period (LP) seismic events associated with movement of fluids (White et al., 2018; Randall et al 2019). Between December 2001 and January 2002 both LP-earthquakes intensified and rock fracturing earthquakes were recorded by IG-EPN. After this episode, the seismic volcanic activity stopped until September 2005 when Volcano Tectonic type (VT) seismic events, characterized by their low seismic intensity, occurred and then declined to background level until 2016.

In April 2016, a large subduction earthquake struck the Manabi coast, offshore Pedernales (Figure 1). With a magnitude $M_w = 7.8$, a general westward displacement centimeters was observed in many GPS stations, including those at Cayambe (Mothes et al., 2019) located 232 km away from the epicenter. This shaking could also have provoked movement on faults and volcanic systems (Nocquet et al., 2016; Mothes et al., 2018; Hernandez et al., 2018). Since June 6th, 2016, a new increase in seismicity corresponding to fracture VT events has been observed in the Cayambe area (Fig. 3). This new increase reached an important peak in June 12-13; and produced a much higher energy release than that observed in 2001-2002. In this period, 2300 earthquakes were recorded, the highest number of events recorded at Cayambe since seismic monitoring began in the late 1980s. According to Butcher et al. (2021), the June swarm was associated with a reactivation of the regional Chingual fault system. Over a few weeks this activity progressively decreased, returning to background level in August, 2016. Shortly afterwards, in September, a new increase in activity was recorded, with the presence of short-duration seismic swarms (VT earthquakes). The location of the September events was beneath Nevado Cayambe central cone, more particularly beneath the southern and western flanks. Two significant VT events, larger than usual, with a magnitude above 3, were recorded on November 14th (M3.3) and 27th (M3.6), respectively. In the last weeks of December 2016, the energy release of events and number of seismic events remained above the normal (average 68 events/day, Fig. 5 in Supplementary Material) for this volcano (Instituto Geofísico - EPN, 2016d; Butcher et al., 2021).

At the beginning of 2017, seismic activity continued similar to the last 6 months of 2016 and since May 2017 a decrease in the number of events was observed. Another swarm occurred in September 2017 with fewer events compared to the beginning of this year. The month with the greatest activity was March with a total of 2723 earthquakes, while the month with the lowest activity was December with 179 earthquakes, for a total of 13140 events registered in 2017. Overall, that year's activity was considered moderately high, especially in February and March. Hypocenter depths reach approximately 10 km, while earthquakes that pertain to

local tectonic activity reached depths close to 30 km below the summit (Instituto Geofísico - EPN, 2017a,b; Butcher et al., 2021).

Concerning 2018, a total of 5696 seismic events were recorded, marking a decrease compared to the number of events in 2017. November was the month with the greatest activity for a total of 834 earthquakes, while the month with the least activity was January with 203 earthquakes. Most of the events were concentrated in the central zone of the volcano and depths did not exceed 20 km below the surface (Instituto Geofísico - EPN, 2018).

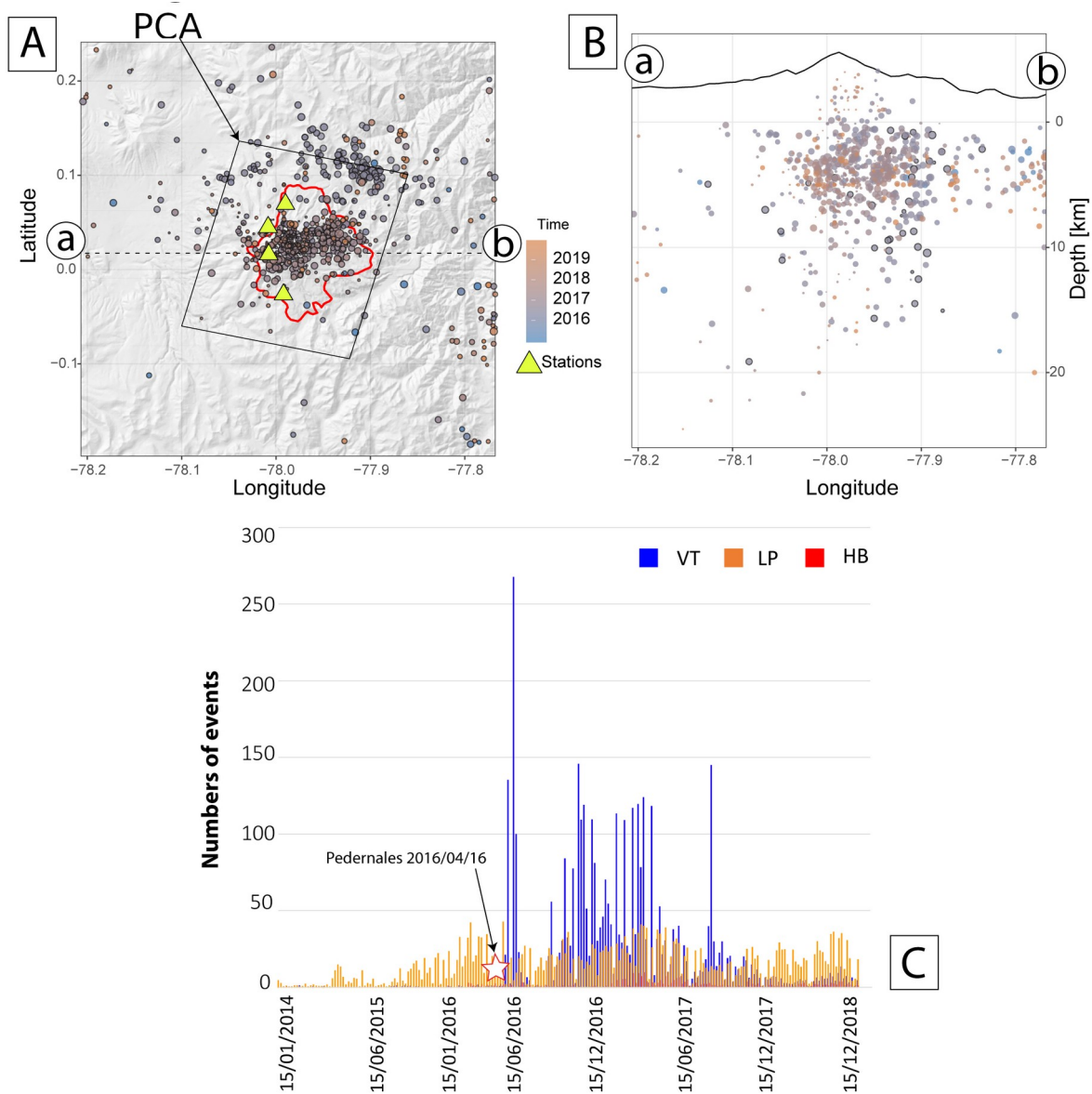


Figure 3. a, b) Top-Locations of seismic events from 10 January 2015 to December 2018. Most events are concentrated between 3 and 10 km below sea level (778 earthquakes between 2015-01-10 - 2018-12-06 with magnitudes between 0.1 - 3.6). c) Cayambe Volcano Seismic activity record from December 2014 to December 2018, VT: volcano tectonic events, LP: low period events and HB: Hybrid events.(Source: Instituto Geofísico - EPN) The red star represent the subduction Pedernales earthquake in April 16, 2016. The box black line in Figure 3 a) outlines the area over which principal component analysis (PCA) has been conducted.

4. SAR data description and processing method

a. Interferogram computation

In order to study surface deformation patterns at Cayambe volcano area, we use an implementation of the Small Baseline Subset (SBAS) strategy, the “New Small Baseline Subset (NSBAS)” processing chain package (Doin et al., 2011), to process the Synthetic Aperture Radar (SAR) dataset provided by Sentinel-1 (C band, wavelength = 5.6 cm). The NSBAS chain ingests Single Look Complex (SLC) radar scenes to obtain interferograms and finally time series of the line of sight (LOS) surface displacement (Doin et al., 2011; Doin et al., 2015; Grandin, 2015). NSBAS has been especially optimized for monitoring transient ground motion of small amplitude, taking place over large areas and in natural settings (Doin et al., 2015).

The Sentinel-1 archive on the descending track with relative orbit number 142 (see footprint on Fig. 1, white square) consists of 104 acquisition dates between October 2014 and November 2018. Continuous SLC images along subswath iw3 have been obtained by cutting burst overlaps in the middle of the overlap region, by stitching the bursts, and by correcting the phase from the effect of antenna azimuth steering within each burst. The combined use of precise orbital data (Peter et al., 2017), of the digital elevation model from the Shuttle Radar Topographic mission (Farr et al., 2007), and of SLC image correlation, allowed co-registering of all images to a reference image geometry. Differential interferograms are generated with 8 looks in range and 2 looks in azimuth. The enhanced spectral diversity technique (Scheiber and Moreira, 2000) was applied on each interferogram to extract a parameterization

of phase jumps across burst boundaries. This parameterization has been inverted into a time series to obtain stable values, before being used to correct differential interferograms. We then correct all interferograms for stratified atmospheric delays using the ERA5 meteorological model from European Centre for Medium-Range Weather Forecast (Hersbach et al., 2020), as described in Doin et al. (2009) and in Jolivet et al. (2011). After this correction, interferograms are filtered to enhance the signal to noise ratio and decrease the impact of decorrelation. Different filter combinations and filter strength have been tested. We found that the optimal combination was to : (1) compute phase colinearity (Pinel-Puysegur et al., 2012), replace interferogram amplitude by the colinearity (as in Daout et al., 2017), before further multilooking by a factor of 2; (2) repeat step (1) to obtain interferograms with 8 looks in azimuth and 32 looks in range; (3) apply a sliding window with a gaussian weight on the wrapped interferogram, and keep, besides the phase, the coherence associated with the gaussian convolution. Then, the unwrapping process begins in the sub-region of the interferogram where the coherence is maximum and propagates to the contiguous areas where coherence is above the threshold, while choosing an optimal path maintaining the coherence as high as possible (Grandin et al., 2012).

b. Transforming the interferogram combination into time series

The inversion of the interferogram network into time series allows us to compute discrepancies between original and reconstructed interferograms, for each pixel and each interferometric couple (Lopez-Quiroz et al., 2009). This led us to identify the main unwrapping errors and to correct them manually wherever possible. A few interferograms were discarded when a proper correction of unwrapping errors was unsuccessful. Remaining unwrapping errors of small spatial extent were automatically corrected as explained in Doin et al. (2011). The root mean square average of the misclosure maps then serves as a proxy for the time series quality and is used, with a threshold of 1 rad, to mask some low-quality pixels.

The choice of the interferogram network is particularly crucial, as it has been shown recently that “fading” signals associated with vegetation can bias the reconstructed time series (Ansari et al., 2021). A first network of 264 short temporal

baseline interferograms (≤ 3 months, Fig. 1a and Fig. 1d in Supplementary Material) was constructed to limit the impact of temporal decorrelation, on top of which 74 one-year and 12 six months interferograms have been added (Fig. 1b and Fig. 1e in Supplementary Material). Several tests have been conducted in order to choose the best interferogram network. Including only small temporal baseline interferograms (≤ 3 months) resulted in strong apparent subsidence in mostly crop areas (Fig. 1g in Supplementary Material). This effect almost completely disappears when one year interferograms are added (Fig. 1h in Supplementary Material). To further assess whether adding one year vintage interferograms was sufficient to remove the bias, we also removed interferograms shorter than one month while keeping long duration interferograms (Fig. 1c, Fig. 1f and Fig. 1i in Supplementary material). The obtained Line Of Sight (LOS) velocity map was then in very good agreement with the preceding one. Note that, on the NC complex itself, the three solutions show consistent LOS velocity patterns, probably because the volcanic complex is characterized by relatively limited temporal decorrelation and the absence of agricultural fields. However, including one year vintage interferogram slightly decreases the amplitude of the velocity pattern on the volcano. In this paper, we choose to present results with the third network, that should be devoid of phase bias.

The last steps have been to estimate the North-South and East-West ramps of all interferograms, to invert them into time series, and then to correct the interferograms from the ramps to obtain “flattened” interferograms. Finally, all interferograms have been referenced in a small and coherent area located close to NC. This finally allows the generation of the LOS velocity map shown in Fig. 2 of Supplementary Material and the time series in the Cayambe Volcano area, shown in Fig. 3 of Supplementary Material.

c. SAR time series post-processing

The phase time series includes mainly two contributions that we aim to separate, the displacement and the residual atmospheric delay. Although interferograms were corrected from the predicted delay using the ERA5 model, and

despite the high elevation of the volcanic structure, residual atmospheric patterns still affect the phase delay maps at each time step. Therefore, in order to extract the most significant deformation pattern on Cayambe volcano, we perform a Principal Component Analysis of the time series on the area of interest. The first component in time is characterized by a linear trend and a step in November 2016, and a spatial component with displacement towards the satellite on the eastern flank of the volcano. This led us to perform a linear decomposition of the phase delay time series as:

$$\text{Phi}(t_i) = a * t_i + b * H(t_i - 2016.85) + c$$

where t_i is the decimal year of each acquisition i , a is the pluri-annual LOS velocity, b is the displacement step occurring in November 2016, H is the Heaviside function and c is a constant. The parameters a , b , and c are obtained by least square inversion for each pixel, with an iteration to downweight acquisitions i with large averaged dispersion around the adjusted function $\text{Phi}(t_i)$.

d. Modeling of the displacement field

We modeled the displacement field retrieved from SAR data analysis using the analytical solution for a point source volume change applied in a homogeneous half-space as defined by Mogi (1958). This four parameters model, which is the simplest and the most widely used in volcanology, provides a robust first order estimation of the 3-D coordinates (position and depth) as well as the strength of the deep perturbation responsible for surface displacement. The model does not take into account the topography of the volcano. A classical Bayesian inversion was performed on the subsampled displacement map following Bagnardi and Hooper (2018) and using the Geodetic Bayesian Inversion Software (GBIS), written in Matlab. During the inversion a constant offset in the line-of-sight direction was estimated, increasing the number of unknown parameters to five.

5. Results

a. Deformation signal

The mean velocity map derived from the SAR time series analysis (Fig. 2 in Supp Mat.) evidences a significant displacement of the ground surface reaching 0.44 cm/yr in LOS and directed towards the satellite. This displacement is located on the southeastern part of the Cayambe volcano flanks and is interpreted as an uplift induced by magma emplacement at depth. From the temporal evolution of the surface displacement field (see Fig. 3 of Supp. Mat.), this uplift may have started in August 2016 and became significant in November 2016. Figure 4 presents the temporal evolution of the amplitude of the first component resulting from the Principal Component Analysis of the SAR time series, this principal component explaining 58% of the signal. It clearly shows that most of the uplift is focused in time and occurs around November 2016, being concomitant with the two $M > 3$ VT events recorded in the seismic swarm about 7 months after the Pedernales earthquake (Fig. 4). From Fig 4b, an uplift trend is probably observed before an observed step and possibly after. However, in the following, we will focus on the sudden displacement recorded during November 2016 as it is the most significant of all. As detailed previously (section 4.b), we performed a linear decomposition of the signal using a Heaviside function with a step defined at 2016.85 corresponding to the 6th November 2016. Figure 5 shows the amplitude of the displacement associated with the step recorded in November 2016. The southeastern part of the edifice shows an important displacement signal. This deformation is also seen around the entire volcano, but in the SE flank the signal is clearer due to the acquisition geometry. For the descending track here considered, horizontal and vertical components of the displacement field induced by an inflating volcano are added on the southeastern flank whereas they are subtracted on the northwestern one. This discrepancy between both flanks appears clearly on both profiles displayed (A-A' and B-B'). The inflation signal reaches ~ 2.5 cm in LOS.

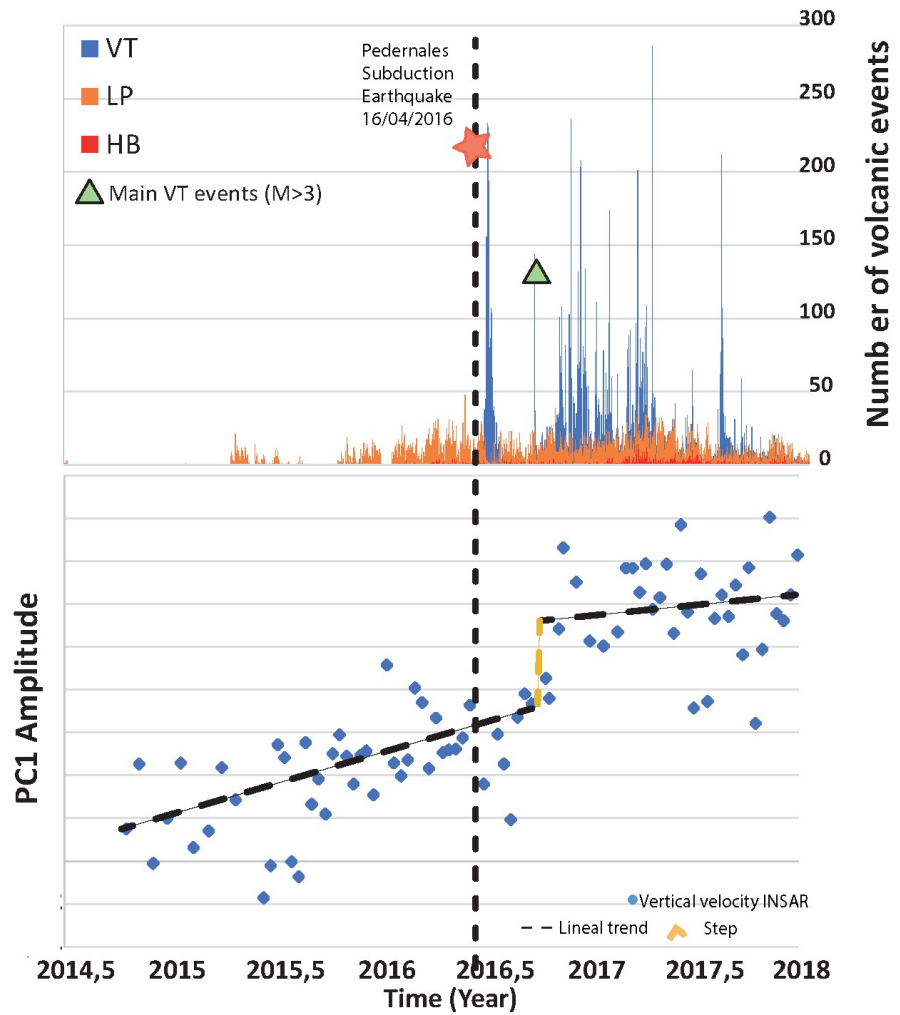


Figure 4. Comparison between the first PCA component in time (bottom panel) and the number of volcanic events between 2014 and 2018 (top panel, as in Figure 3). The orange and black dashed lines, sketched by hand, underline the significant signal increase between mid-2016 and mid-2017 related to the seismic activity increase. The star shows the date of the Pedernales Subduction Earthquake. The green triangle shows the main VT events occurring at the volcano in November 2016 ($M > 3$).

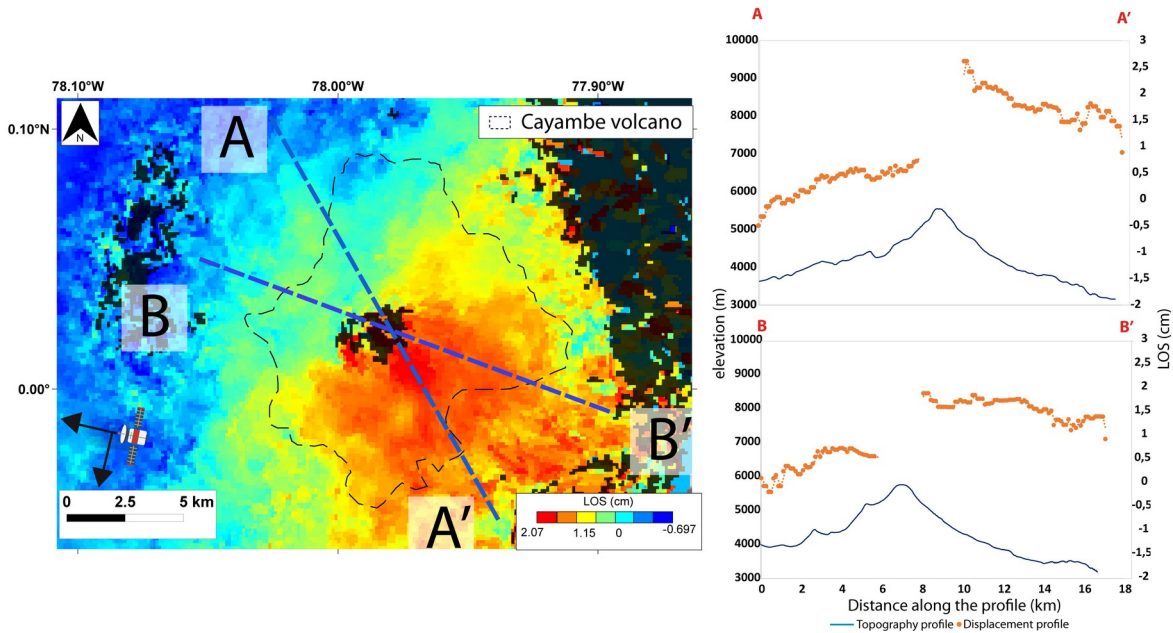


Figure 5. LOS displacement field of Cayambe Volcano corresponding to the step amplitude (parameter b in equation (1)) of the linear decomposition and occurring in November 2016. On the right panel, elevation and LOS displacement are displayed for two profiles located by dashed blue lines on the displacement field map.

b. Mogi source modeling

We inverted the displacement field corresponding to the step of the linear decomposition (displayed in Fig. 5) for a volume change at depth using a Mogi model as described in section 4.c. The subsampled displacement field was composed of 339 data points. The optimal (maximum a posteriori probability) model derived from the Bayesian inversion was obtained at 0.0148°N , 77.9613°W located 6133 m beneath the surface, with a volume change of 2.63 million m^3 (see Fig. 6 and Table 1 for inversion

input parameters and results). Note that the uncertainty on the depth remains relatively large and the volume change of magma is expected to increase with the depth of emplacement (see Fig 4 of Supp. Mat.). The offset in LOS is estimated around 6 mm.

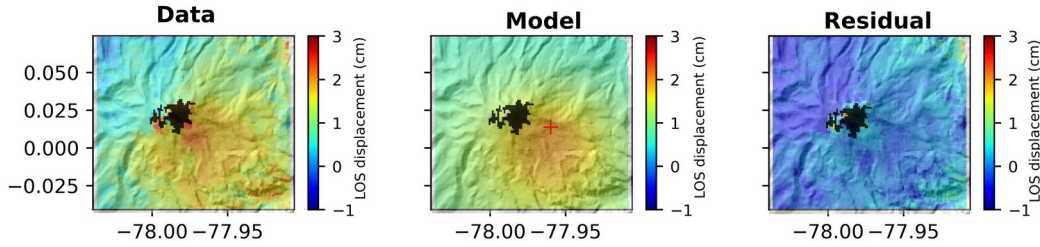


Figure 6. Displacement field recorded at Cayambe volcano in November 2016 (in LOS) from (left), (middle) optimal Mogi model, and (right) residuals between data and model (black dashed line corresponds to the Cayambe volcano area). The model corresponds to a Mogi source located 6133 m beneath the surface (red cross), inflating with the entry of 2.63 millions of m^3 .

Parameters	Input value and Prior	Maximum a posteriori solution	2.5 percentiles of posterior PDFs	97.5 percentiles of posterior PDFs
X (m)	[-8000;6000]	2998.3	2076.1	4902.1
Y (m)	[-7000;-6000]	-535.5	-1257.3	637.1
Depth (m)	[100;20000]	6133	4727	10949
DV (Mm3)	[-1e7;1e7]	2.63	1.47	9.56

Table 1: Inversion parameters and results. Positions (X and Y) are expressed in distance from the grid center located at 0.0193 °N, 77.98°W (m).

6 . Discussion and Conclusions

The NSBAS processing chain developed at ISTerre for time series analysis of SAR data has proven efficient to evidence a previously undetected uplift event taking place at Cayambe volcano possibly through the whole studied period, 2014-2018, but mostly in November 2016, about 7 months after the Pedernales subduction

earthquake. Such large-scale (around 10 km in radius) inflation had never been documented at Cayambe volcano which hasn't erupted for more than two centuries. We attribute this local uplift to pressure increase around 6 km beneath the surface. Magma emplacement at this depth seems consistent both with the petrological data reported by Samaniego (2001) and Samaniego et al. (2005), who suggests that amphibole crystallization pressures occurred at 18 MPa (6.6 ± 1.5 km below the summit); and with relocation of seismic swarm (Butcher et al., 2021) that point out to VT hypocenters at >6 km below the summit.

SAR data are particularly useful in this case where the sparse GPS and tiltmeters network was not able to evidence significant surface deformation. Our study confirms the interpretation of Butcher et al. (2021) of the late seismic part of the VT seismic swarm located on the flank of the Cayambe volcano edifice being induced by magma ascent. The decrease in seismic activity and deformation after the end of 2017 could indicate that the limited volume of magma emplaced prevented any further ascent towards the surface, but a new inflow in the coming years could build on this event and promote an eruption in the future.

The NSBAS processing chain thus allows studying the surface deformation patterns of the Cayambe volcanic complex, despite its highly variable geomorphic features, ice cap, different vegetation type (on the eastern Amazonian side compared with the western interandean side), varying size of watersheds with different atmospheric effects. These results obtained in a volcanic, vegetated and compressional setting are promising and should promote the generalization of the use of Sentinel-1 data set for operational volcanoes monitoring, especially in the Andes.

The relationship between megathrust tectonic earthquakes and volcanic activity in the far field overriding crust remains a striking question in Earth sciences, mainly due to the lack of observational data. Large earthquakes can affect volcanic areas within the continental region located at hundreds of kilometers away from the epicenter, inducing swarms of earthquakes, ground deformation, migration of magmatic gasses, excitation of geothermal activity and even possibly triggering eruptions (e. g. Linde & Sacks, 1998; Hill et al., 2002; Watt et al., 2009; Walter and Amelung, 2007; Namiki et al. 2018). Recent illustrations of the susceptibility of

volcanic zones, characterized by the presence of fluids at depth, to be influenced and/or destabilized by large subduction earthquakes include the Maule 2010, Chile earthquake (Pritchard et al., 2013; Li et al., 2017) and Tohoku 2011 earthquake in Japan (Takada et al., 2013; Brenguier et al., 2014; Ishitsuka et al., 2017). As triggering can occur either through dynamic or static stress variations, or through cascading events and/or results from fluid migration, the induced volcanic unrest can be either almost instantaneous or delayed by several months, the wide range of timescale involved making it more difficult to identify and characterize the phenomenon.

The geophysical observations recorded at Cayambe volcano in Ecuador provide new insight into the potential influence of regional tectonics on volcanoes behavior. The Pedernales earthquake on April 16, 2016 (Mw 7.6) caused tectonic strain changes in volcanic centers within the NAS, in the inter-Andean valley as evidenced for instance at Guagua Pichincha volcano (Hernandez et al., 2018). Seismic activity at Guagua Pichincha located at 12 km distance from Quito city, is typically characterized by recurrent, short duration seismic swarms recorded by a network of short-period and broad-band seismometers. A reactivation of seismic swarms was observed as a result of the Pedernales earthquake and interpreted as due to a widespread volumetric expansion within the NAS induced by the subduction earthquake (Hernandez et al., 2018). A significant increase in seismic activity also occurred in the vicinity of Cayambe Volcano. It started in June with distal seismicity located north of Cayambe Volcanic Complex. This June swarm was interpreted as resulting from stress perturbations and displacements induced on the CCPP by the Pedernales earthquake (Butcher et al, 2021). This first phase of seismic unrest was followed by a second one starting in September on the volcano flanks and culminating in two M>3 events in November 2016. The uplift recorded in November 2016 proves that magma emplacement 6 km below the surface was probably causing this second VT swarm.

The triggered unrest of the Cayambe volcano is probably directly linked to its location near/on to the CCPP NAS tectonic boundary, expected to accommodate partitioning of the oblique convergence and strain within the South American upper plate with respect to the subducting Nazca/Cocos plates. This process has been invoked, for instance, in Chile for the Chiloe forearc sliver (Wang et al., 2007) or

Central America (La Femina et al., 2009) where the major fault system accommodating the oblique convergence runs along the active volcanic arc. Most of the active volcanic arc in Ecuador lies west of the narrow CCPP tectonic limit but the Cayambe volcano lies the closest to the northern CCPP Chingual segment.

It seems that the location of Cayambe Volcano in proximity to the CCPP fault system at the boundary of the NAS makes it prone to be strongly influenced by subduction earthquakes. Being active, potentially explosive and covered by an ice cap, its high-sensibility to large earthquakes should be taken into account in local hazard assessment as a large eruption near the summit would melt ice and snow, resulting in lahars, which might be directed toward the town of Cayambe and adjacent inhabited areas, potentially impacting more than 30000 people and Ecuador's largest hydroelectric plant situated along Cayambe's eastern drainage network.

6. Acknowledgments

This research was supported by SENECYT (Secretaría de Educación Superior, Ciencia, Tecnología e Innovación, Programa de Becas Internacionales de Posgrado 2018, Ecuador), IDEX (Initiatives-Science – Innovation –Territoires – Economie), IRD (the French National Research Institute for Sustainable Development), the Instituto Geofísico de la Escuela Politécnica Nacional (IG-EPN, Ecuador) through the Laboratoire Mixte International “Séismes et Volcans dans les Andes du Nord”. This work is also supported by the Centre National d’Etude Spatiale (CNES) of France through the program APR CNES and was part of P. A. Espín Bedón master studies at Grenoble Alpes University.

We thank the Programme National de Teledétection Spatiale (PNTS) of French CNRS for its support through the "TRIPLETS" project (PI Doin).

This was carried out at ISTERre, which is part of Labex International efforts @ OSUG and benefited from CIMENT computing center facilities. We thank the “Seismic cycle and transient deformations” staff from ISTERre and Instituto Geofísico - EPN staff for helping with the data and for providing useful comments. Sentinel-1 data from the Copernicus Sentinel program were provided by the European Space Agency and have

been downloaded from CNES-PEPS (Sentinel Products Operating Platform, <https://peps.cnes.fr>).

7. Reference:

Ansari, H., De Zan, F. and Parizzi, A., 2021. Study of Systematic Bias in Measuring Surface Deformation With SAR Interferometry, *IEEE Transactions on Geoscience and Remote Sensing* 59, 1285-1301. <https://doi.org/10.1109/TGRS.2020.3003421>.

Alvarado, A., L. Audin, J. M. Nocquet, E. Jaillard, P. Mothes, P. Jarrín, M. Segovia, F. Rolandone, and D. Cisneros, 2016. Partitioning of oblique convergence in the northern Andes subduction zone : migration history and present-day boundary of the North Andean Sliver in Ecuador, *Tectonics*, 35, <https://doi.org/10.1002/2016TC004117>.

Bablon, M., Quidelleur, X., Samaniego, P., Le Pennec, J.-L., Audin, L., Jomard, H., Baize, S., Liorzou, C., Hidalgo, S., Alvarado, A., 2019. Interactions between volcanism and geodynamics in the southern termination of the Ecuadorian arc, *Tectonophysics* 751, 54-72. <https://doi.org/10.1016/j.tecto.2018.12.010>.

Bagnardi, M., Hooper, A., 2018. Inversion of surface deformation data for rapid estimates of source parameters and uncertainties: A Bayesian approach. *Geochemistry Geophysics Geosystems* 19. <https://doi.org/10.1029/2018GC007585>.

Battaglia, M., Cervelli, P., Murray, J., 2013. dMODELS: A MATLAB software package for modeling crustal deformation near active faults and volcanic centers, *Journal of Volcanology and Geothermal Research* 254, 1-4. <https://doi.org/10.1016/j.jvolgeores.2012.12.018>.

Bernard, B., Andrade, D., 2011. "Volcanes cuaternarios del Ecuador continental", IG-EPN Poster Informativo.

Biggs, J., Mothes, P., Ruiz, M., Amelung, F., Dixon, T. H., Baker, S., and Hong, S.H., 2010. Stratovolcano growth by co-eruptive intrusion: The 2008 eruption of Tungurahua Ecuador, *Geophysical Research Letters* 37, 1-5. <https://doi.org/10.1029/2010GL044942>.

Biggs, J., Robertson, E., Cashman, K. V., 2016. The lateral extent of volcanic interactions during unrest and eruption. *Nature Geoscience* 9, 308-311. <https://doi.org/10.1038/ngeo2658>.

Biggs, J., Pritchard, M. E., 2017. Global volcano monitoring : What does it mean when volcanoes deform ?, *Elements* 13, 17–22. <https://doi.org/10.2113/gselements.13.1.17>.

Biggs, J., Wright, T.J., 2020. How satellite InSAR has grown from opportunistic science to routine monitoring over the last decade, *Nature Communication* 11, <https://doi.org/10.1038/s41467-020-17587-6>.

Butcher, S., Bell, A.F., Hernandez S., and Ruiz, M., 2021. Evolution of Seismicity During a Stalled Episode of Reawakening at Cayambe Volcano, Ecuador. *Frontier in Earth Science* 9. <https://doi.org/10.3389/feart.2021.680865>.

Cáceres, B., 2010. Actualización del inventario de tres casquetes glaciares del Ecuador. Informe de Pasantía de Investigación en Université Nice Sophia Antipolis.

Champenois, J., Pinel, V., Baize, S., Audin, L., Jomard, H., Hooper, A., Alvarado, A. and Yepes, H., 2014. Large-scale inflation of Tungurahua volcano (Ecuador) revealed by Persistent Scatterers SAR interferometry, *Geophysical Research Letters* 41. <https://doi.org/10.1002/2014GL060956>.

Daout, S., Doin, M.-P., Peltzer, G., Socquet, A., Lasserre, C., 2017. Large-scale InSAR monitoring of permafrost freeze-thaw cycles on the Tibetan Plateau. *Geophysical Research Letters* 44, 901–909. <https://doi.org/10.1002/2016GL070781>.

Doin, M. P., Lasserre, C., Peltzer, G., Cavalié, O., Doubre, C., 2009. Corrections of stratified tropospheric delays in SAR interferometry: Validation with global atmospheric models. *Journal of Applied Geophysics* 69, 35–50. <https://doi.org/10.1016/j.jappgeo.2009.03.010>.

Doin, M.-P., Lodge, F., Guillaso, S., Jolivet, R., Lasserre, C., Ducret, G., Grandin, R., Pathier, E., Pinel, V., 2011. Presentation of the small baseline NSBAS processing chain on a case example: The Etna deformation monitoring from 2003 to 2010 using Envisat data, paper ESA SP-697 presented at Fringe 2011 Symposium, Frascati, Italy, 19–23 Sept 2011, 3434-3437.

Doin, M.-P., Twardzik, C., Ducret, G., Lasserre, C., Guillaso, S., Jianbao S., 2015. InSAR measurement of the deformation around Siling Co Lake: Inferences on the lower crust

viscosity in Central Tibet, *Journal Geophysical Research Solid Earth* 120, 5290–5310. <https://doi.org/10.1002/2014JB011768>.

Ebmeier, S. K., Biggs, J., Mather, T. A. and Amelung, F., 2013. Applicability of InSAR to tropical volcanoes: insights from Central America, *Geological Society of London Special Publications*, 380, Remote-sensing of volcanoes and volcanic processes: Integrating observation and modelling. <https://doi.org/10.1144/SP380.2>.

Ebmeier, S.K., Andrews, B.J., Araya, M.C., Arnold, D.W.D., Biggs, J., Cooper, C., Cottrell, E., Furtney, M., Hickey, J., Jay, J., 2018. Synthesis of global satellite observations of magmatic and volcanic deformation: Implications for Volcano monitoring & the lateral extent of magmatic domains. *Journey Applied Volcanology* 7, 1–26. <https://doi.org/10.1186/s13617-018-0071-3>.

Farr, T. G., Rosen, P. A., Caro, E., Crippen, R., Duren, R., Hensley, S., Kobrick, M., Paller, M., Rodriguez, E., Roth, L., 2007. The shuttle radar topography mission. *Reviews of geophysics* 45. <https://doi.org/10.1029/2005RG000183>.

Global Volcanism Program, Report on Cayambe (Ecuador) (Wunderman, R. ed.), (2006), *Bulletin of the Global Volcanism Network*, 31:11. Smithsonian Institution, <https://doi.org/10.5479/si.GVP.BGVN200611-352006>.

Grandin, R., Doin, M.-P., Bollinger, P., Pinel-Puysségur, P., Ducret, G., Jolivet, R., Sapkota, S.N., 2012. Long-term growth of the Himalaya inferred from interseismic InSAR measurement, *Geology* 40, 1059-1062. <https://doi.org/10.1130/G33154.1>.

Grandin, R., 2015. Interferometric Processing of SLC Sentinel-1 TOPS Data, processing of the 2015 ESA Fringe workshop, ESA Special Publication, SP-731, Frascati Italy.

Hall, M. L., Bernardo B., 1991. El volcanismo plio-cuaternario en los Andes del Ecuador." *Estudios Geograficos* 4, 5-38.

Hernandez, S., Ruiz, M.C., 2018. Earthquake-Volcano Conversations at Volcan Guagua Pichincha, Ecuador. *Seismological Research Letters* 89, 717–966. <https://doi.org/10.1785/0220180082>.

Instituto Geofísico-Escuela Politécnica Nacional (IGEPN), 2016a. Informe Especial – Volcán Cayambe N°1. Consultado el 04/01/2017 disponible en: <http://www.igepn.edu.ec/cayambe-informes/cay-especiales/cay-e-2016/15310-informe-especial-volcan-cayambe-n-1/file>

Instituto Geofísico-Escuela Politécnica Nacional (IGEPN), 2016b. Informe Especial – Volcán Cayambe N°2. Consultado el 04/01/2017 disponible en: <http://www.igepn.edu.ec/cayambe-informes/cay-especiales/cay-e-2016/16585-informe-especial-volcan-cayambe-n-2/file>

Instituto Geofísico-Escuela Politécnica Nacional (IGEPN), 2016c. Informe Especial – Volcán Cayambe N°3. Consultado el 04/01/2017 disponible en: <http://www.igepn.edu.ec/cayambe-informes/cay-especiales/cay-e-2016/16567-informe-especial-volcan-cayambe-n-3/file>

Instituto Geofísico-Escuela Politécnica Nacional (IGEPN), 2016d. Informe Especial – Volcán Cayambe N°4. Consultado el 04/01/2017 disponible en: <http://www.igepn.edu.ec/cayambe-informes/cay-especiales/cay-e-2016/16657-informe-especial-volcan-cayambe-n-4/file>

Instituto Geofísico-Escuela Politécnica Nacional (IGEPN), 2016e. Informe Especial – Volcán Cayambe N°5. Consultado el 04/01/2017 disponible en: <http://www.igepn.edu.ec/cayambe-informes/cay-especiales/cay-e-2016/16780-informe-especial-volcan-cayambe-n-5/file>

IGEPN, 2017a. Informe Especial – Volcán Cayambe N°1. Consultado el 04/04/2017 disponible en: <http://www.igepn.edu.ec/cayambe-informes/cay-especiales/cay-e-2017/17196-informe-especial-volcan-cayambe-n-1-1/file>

Instituto Geofísico-Escuela Politécnica Nacional (IGEPN), 2017b. Informe Especial – Volcán Cayambe N°2. Consultado el 04/04/2017 disponible en: <http://www.igepn.edu.ec/cayambe-informes/cay-especiales/cay-e-2017/17425-informe-especial-volcan-cayambe-n-1-2/file>.

Instituto Geofísico-Escuela Politécnica Nacional (IGEPN), 2018. Informe Anual 2018 – Volcán Cayambe: Consultado el 05/11/2021 disponible en: <http://www.igepn.edu.ec/servicios/busqueda-informes>.

Hersbach, H., Bell, B., Berrisford, P., Hirahara, S., Horányi, A., Muñoz-Sabater, J., Peubey, C., Nicolas, J., Radu, R., Schepers, D., Simmons, A., Soci, C., Abdalla, S., Abellan, X., Balsamo, G., Bechtold, P., Biavati, G., Bidlot, J., Bonavita, M., De Chiara, G., Dahlgren, P., Dee, D., Diamantakis, M., Dragani, R., Flemming, J., Forbes, R., Fuentes, M., Geer, A., Haimberger, L., Healy, S., Hogan, R.J., Hólm, E., Janisková, M., Keeley, S., Laloyaux, P., Lopez, P., Lupu, C., Radnoti, G., Rosnay, P., Rozum, I., Vamborg, F., Villaume, S., Thépaut,

J.N., 2020. The ERA5 global reanalysis. Quarterly Journal of the Royal Meteorological Society 146, 1999-2049. <https://doi.org/10.1002/qj.3803>.

Hill, D. P., M., Pollitz, F., Newhall, C., 2002. Earthquake-Volcano Interactions, Physics Today, 41-47. <https://doi.org/10.1063/1.1535006>.

Ishitsuka, K., Matsuoka, T., Nishimura, T., Tsuji, T., ElGrarbawi, T., 2017. Ground uplift related to permeability enhancement following the 2011 Tohoku earthquake in the Kanto Plain, Japan, Earth, Planets and Space, 69-81. <https://doi.org/10.1186/s40623-017-0666-7>.

Jolivet, R., Grandin, R., Lasserre, C., Doin, M.-P., Peltzer, G., 2011. Systematic InSAR tropospheric phase delay corrections from global meteorological reanalysis data. Geophysical Research Letters 38. <https://doi.org/10.1029/2011GL048757>.

La Femina, P., Hugh Dixon, T., Govers, R., Norabuena, E., Turner, H., Saballos, J., Mattioli, G., Protti, M., Strauch, W., 2009. Fore-arc motion and Cocos Ridge collision in Central America., Geochemistry, Geophysics, Geosystems 10.5. <https://doi.org/10.1029/2008GC002181>.

Li, S., Moreno, M., Bedford, J., Rosenau, M., Heidbach, O., Melnick, D., Oncken, O., 2017. Postseismic uplift of the Andes following the 2010 Maule earthquake: Implications for mantle rheology, Geophysical Research Letter 44, 1768–1776. <https://doi.org/10.1002/2016GL071995>.

Lopez-Quiroz P. , Doin, M.-P., Tupin, F., Briole, P., Nicolas, J.-M., 2009. Time series analysis of Mexico city subsidence constrained by radar Interferometry, Journal of Applied Geophysics 69, 1-15, <https://doi.org/10.1016/j.jappgeo.2009.02.006>.

Mogi, K., 1958. Relations between the eruptions of various volcanoes and the deformations of the ground surfaces around them. Bulletin Earthquake Research Institute University Tokyo 36, 99–134.

Mothes, P.A., Rolandone, F., Nocquet, J., Jarrin, P.A., Alvarado, A.P., Ruiz, M.C., Cisneros, D., Páez, H.M., Segovia, M., 2018. Monitoring the Earthquake Cycle in the Northern Andes from the Ecuadorian cGPS Network. Seismology Research Letter 89, 534–541. <https://doi.org/10.1785/0220170243>.

Namiki, A., Rivalta, E., Woith, H. Willey, T., Parolai, S., Walter, T., 2018. Volcanic activities triggered or inhibited by resonance of volcanic edifices to large earthquakes. Geology 47, 67-70. <https://doi.org/10.1130/G45323.1>.

Nocquet, J.-M., Jarrin, P., Vallée, M., Mothes, P.A., Grandin, R., Rolandone, F., Delouis, B., Yepes, H., Font, Y., Fuentes, D., Régnier, M., Laurendeau, A., Cisneros, D., Hernandez, S., Sladen, A., Singaicho, J.-C., Mora, H., Gomez, J., Montes, L., Charvis, P., 2017. Supercycle at the Ecuadorian subduction zone revealed after the 2016 Pedernales earthquake. *Nature Geoscience* 10, 145–149. <https://doi.org/10.1038/ngeo2864>.

Pepe A., Calò F., 2017. A Review of Interferometric Synthetic Aperture RADAR (InSAR) Multi-Track Approaches for the Retrieval of Earth's Surface Displacements. *Applied Sciences* 7, 1264. <https://doi.org/10.3390/app7121264>.

Peter, H., Jäggi, A., Fernández, J., Escobar, D., Ayuga, F., Arnold, D., Wermuth, M., Hackel, S., Otten, M., Simons, W., Visser, P., Hugentobler, U., Féménias, P., 2017. Sentinel-1A–First precise orbit determination results. *Advances in space research* 60, 879-892. <https://doi.org/10.1016/j.asr.2017.05.034>.

Pinel, V., Poland, M., Hooper, A., 2014. Volcanology : Lessons learned from Synthetic Aperture Radar imagery, *Journal Volcanology Geothermal Research*, 81-113. <https://doi.org/10.1016/j.jvolgeores.2014.10.010>.

Pinel-Puysségur, B., Michel, R., Avouac, J.-P., 2012. Multi-link InSAR time series: Enhancement of a wrapped interferometric database. *IEEE Journal of Selected Topics in Applied Earth Observations and Remote Sensing* 5, 784–794. <https://doi.org/10.1109/JSTARS.2012.2196758>.

Pritchard, M.E., Jay, J.A., Aron, F., Henderson, S.T., Lara, L.E., 2013. Subsidence at southern Andes volcanoes induced by the 2010 Maule, Chile earthquake, *Nature Geoscience*, 632-636. <https://doi.org/10.1038/ngeo1855>.

Pritchard, M. E., Biggs, J., Wauthier, C., Sansosti, E., Arnold, D. W. D., Delgado, F., Ebmeier, S. K., Henderson, S. T., Stephens, K., Cooper, C., Wnuk, K., Amelung, F., Aguilar, V., Mothes, P., Macedo, O., Lara, L. E., Poland, M. P., Zoffoli, S., 2018. Towards coordinated regional multi-satellite InSAR volcano observations : results from the latin america pilot project, *Journal of Applied Volcanology* 7, 5. <https://doi.org/10.1186/s13617-018-0074-0>.

Saltogianni, V., Stiros, S., 2012. Modeling the Mogi magma source centre of the Santorini (Thera) volcano, Aegean Sea, Greece, 1994-1999, based on a numerical-topological approach, 1037. <https://doi.org/10.1007/s11200-012-0408-z>.

Samaniego, P., Monzier, M., Robin, C., Hall, M. L., 1998. Late Holocene eruptive activity at Nevado Cayambe Volcano, Ecuador. *Bulletin of Volcanology* 59, 451-459, <https://doi.org/10.1007/s004450050203>.

Samaniego, P., 2001. Transition entre magmatismes calcoalcalinet adakitique dans le cas d'une subduction impliquant une ride océanique: Le volcan Cayambe (Equateur) [Ph.D. thesis]: Clermont- Clermont-Ferrand, Université Blaise Pascal, 305 pp.

Samaniego, P., Eissen, J-P., Monzier, M., Robin, C., Alvarado, A., Yepes, H., 2004. Los peligros volcánicos asociados con el Cayambe. Instituto Geofísico, Quito, 95.

Samaniego, P., Martin, H., Monzier, M., Robi, C., Fornari, M., Eissen, J-P., Cotten, J., 2005. Temporal Evolution of Magmatism in the Northern Volcanic Zone of the Andes: The Geology and Petrology of Cayambe Volcanic Complex (Ecuador), *Journal of Petrology Advance*, 2225–2252. <https://doi.org/10.1093/petrology/egi053>.

Santamaría, S., 2017. Catálogo de eventos volcánicos ocurridos en el Ecuador continental desde el Plioceno y análisis de la frecuencia eruptiva, Tesis de Ingeniería Geológica Escuela Politécnica Nacional Quito-Ecuador, 166. <http://bibdigital.epn.edu.ec/handle/15000/17061>.

Scheiber, R., Moreira, A., 2000. Coregistration of interferometric SAR images using spectral diversity. *IEEE Transactions on Geoscience and Remote Sensing* 38, 2179–2191. <https://doi.org/10.1109/36.868876>.

Simons, M., Rosen, P.A., 2015. Interferometric Synthetic Aperture Radar Geodesy, In Gerald Schubert *Treatise on Geophysics* 3, Elsevierp, 339-385. <https://doi.org/10.1016/B978-044452748-6.00059-6>.

Takada, Y., Fukushima, Y., 2013. Volcanic subsidence triggered by the 2011 Tohoku earthquake in japan. *Nature Geoscience* 6, 637-641. <https://doi.org/10.1038/ngeo1857>.

Valade, S., Ley, A., Massimetti, F., D'Hondt, O., Laiolo, M., Coppola, M., Loibl, D., Hellwich, O., Walter, T.R., 2019. Towards global volcano monitoring using multisensor sentinel missions and artificial intelligence: the MOUNTS monitoring system. *Remote Sensing* 11, 1528. <https://doi.org/10.3390/rs11131528>.

Vizuite, N., Bernard, B., Samaniego, P., 2019. Geochronology, eruptive source parameters and dynamism of the “San Marcos” event at Nevado Cayambe Volcano,

Ecuador. In: Abstract volume of the 8th International Symposium on Andean Geodynamics. Quito, Ecuador. <https://hal.uca.fr/hal-02544337>.

Walter, T.R., Amelung, F., 2007. Volcanic eruptions following $M \geq 9$ megathrust earthquakes: Implications for the Sumatra-Andaman volcanoes: *Geology* 35, 539–542. <https://doi.org/10.1130/G23429A.1>.

Wang, K., Hu, Y., Bevis, M., Kendrick, E., Smalley Jr, R., Vargas, R. B., Lauría, E., 2007. Crustal motion in the zone of the 1960 Chile earthquake: Detangling earthquake-cycle deformation and forearc-sliver translation. *Geochemistry, Geophysics, Geosystems*, 8. <https://doi.org/10.1029/2007GC001721>.

Watt, S. F. L., Pyle, D. M., Mather, T. A., 2009. The influence of great earthquakes on volcanic eruption rate along the Chilean subduction zone. *Earth Planet Science Letter* 277, 399-407. <https://doi.org/10.1016/j.epsl.2008.11.005>.

White, R., McCausland, W., 2016. Volcano-Tectonic Earthquakes: A New Tool for Estimating Intrusive Volumes and Forecasting Eruptions. *Journal Volcanology and Geothermal Research* 309, 139–155. <https://doi.org/10.1016/j.jvolgeores.2015.10.020>.

White, R.A., McCausland, W.A., 2019. A process-based model of pre-eruption seismicity patterns and its use for eruption forecasting at dormant stratovolcanoes, *Journal of Volcanology and Geothermal Research* 382, 267-297. <https://doi.org/10.1016/j.jvolgeores.2019.03.004>.

Yepes, H. , L. Audin, A. Alvarado, C. Beauval, J. Aguilar, Y. Font, and F. Cotton, 2016). A new view for the geodynamics of Ecuador : implication in seismogenic sources definition and seismic hazard assessment, *Tectonics*, 35, <https://doi.org/10.1002/2015TC003941>.

7. Supplementary Material

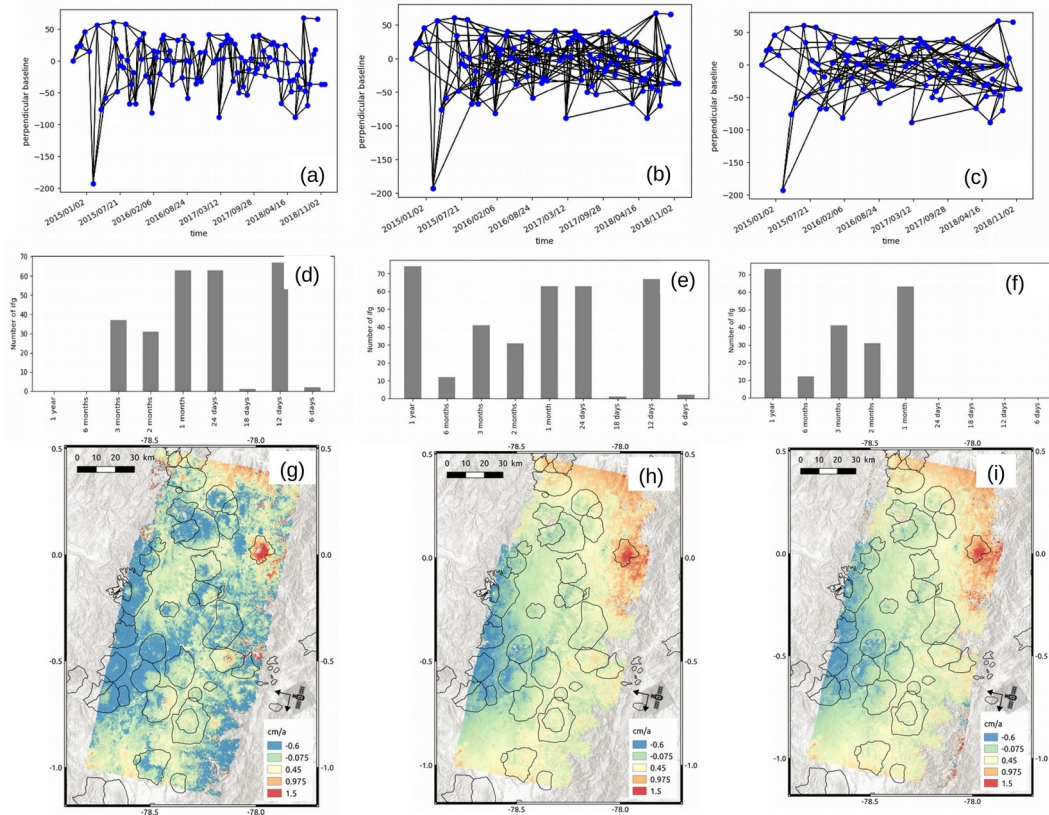


Figure 1. Effect of the chosen interferogram network on the final velocity field. Panels (a-c): Interferometric networks. Each black line represents an interferogram calculated between two SAR images acquired at different dates (dots). Panels (d-f): Distribution of the temporal baseline of the selected interferograms. Panels (g-i): Resulting LOS velocity maps, positive towards satellite. The contours of the volcanoes in the area are shown as black lines. Left column (a,d,g): with only short temporal baseline interferograms. Middle column (b,e,h): with added long duration interferograms. Right column (c,f,i): excluding the shortest temporal baselines.

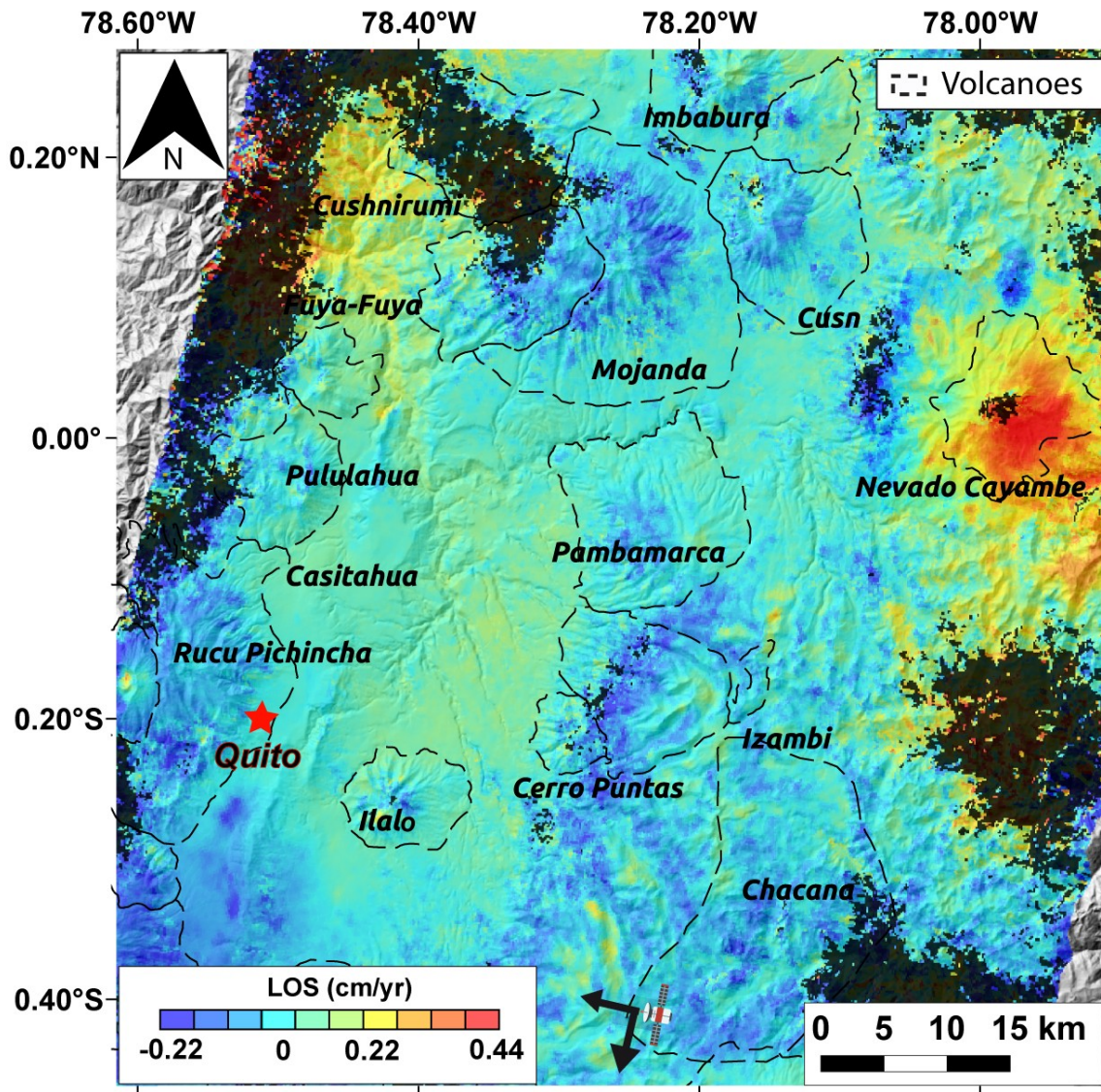


Figure 2. Mean velocity map in the Line of Sight for the entire area, after removal of east-west and north-south ramps. The velocity is expressed in cm/year and positive for surface displacements towards the satellite. The contours of the volcanoes in the area are shown as black dotted lines.

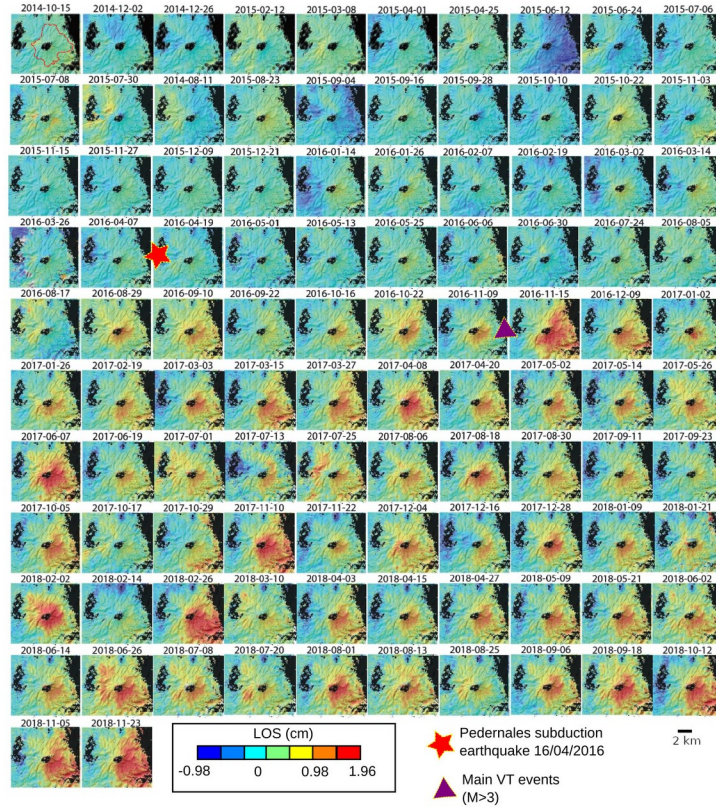


Figure 3. Cumulative line-of-sight displacement over Cayambe volcano, from October 2014 to November 2018. Displacements are relative to the first image (in centimeters) and plotted on 30 meters shadow DEM. The red star and the purple triangle mark the timing of, respectively, the Pedernales earthquake and the two $M>3$ seismic events located on the volcano flank.

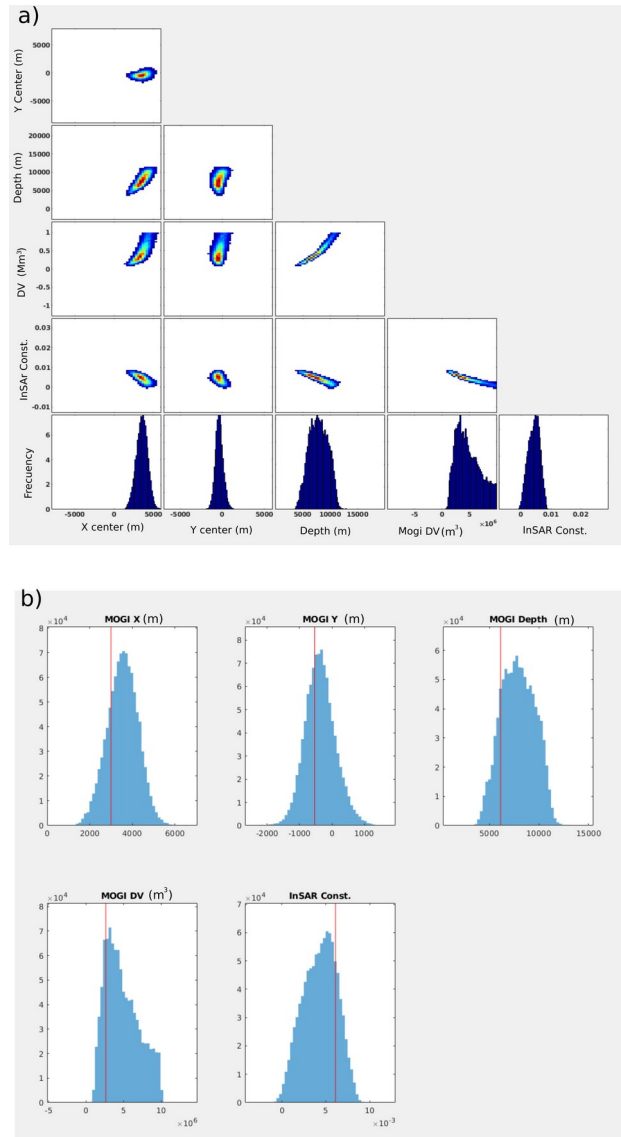


Figure 4. a) Joint probabilities of the Mogi model parameters for Cayambe Volcano, scatter plots are contoured according to frequency (cold colors for low frequency, warm colors for high frequency) and b) Histograms showing the posterior density functions for all source model parameters (blue bars) are plotted together with the optimal values (red lines). Results presented are obtained setting the burning time to 5000.

Cayambe Volcano Seismicity between 1988 and 2020

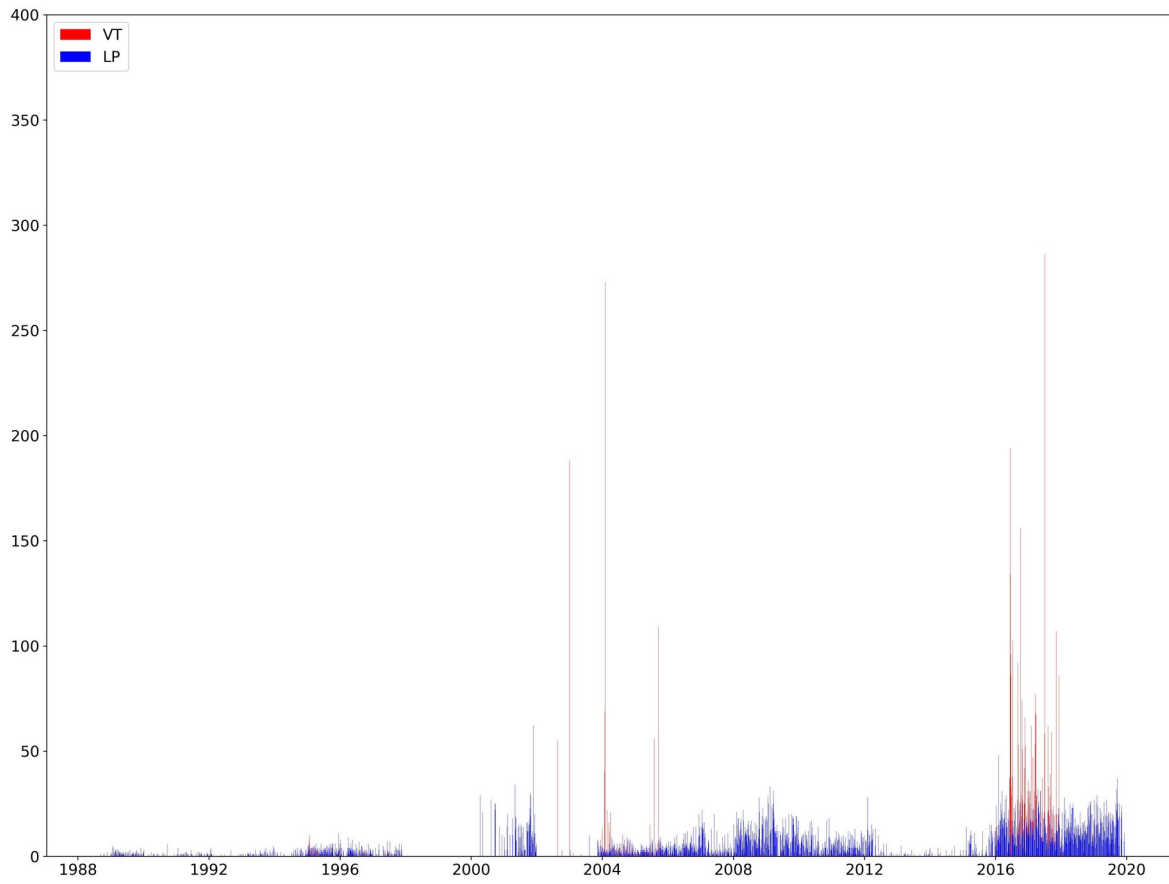


Figure 5. Seismic activity recorded at Cayambe volcano from 1989 to 2020.